MASTER THESIS

Prediction of the nonlinear dynamic behaviour of a concrete slab subjected to blast load

Appendix III – Validation experiment 3

Author: L. Kraaijenbrink

Status: Final

Date: 11 July 2022

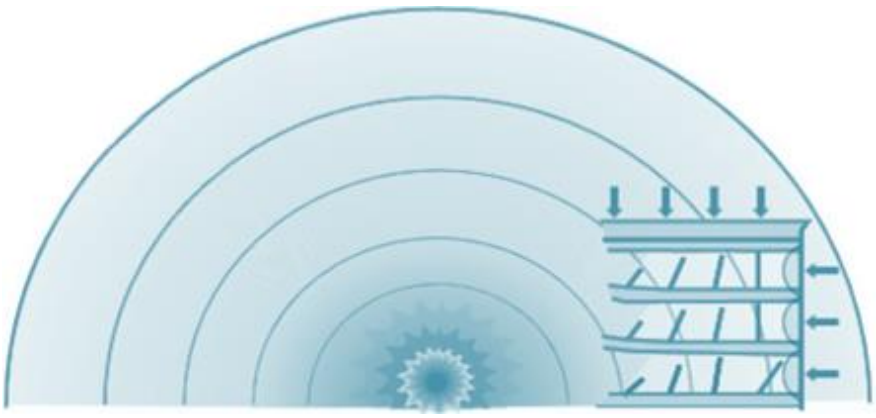

TU Delft

Royal HaskoningDHV
Enhancing Society Together

Open

HASKONINGDHV NEDERLAND B.V.

George Hintzenweg 85
3068 AX Rotterdam
Industry & Buildings
Trade register number: 56515154

+31 88 348 90 00 **T**
info@rhdhv.com **E**
royalhaskoningdhv.com **W**

Document title: Prediction of the nonlinear dynamic behaviour of a concrete slab subjected to blast load

Subtitle: Appendix III – Validation experiment 3

Status: 1.0/Final

Date: 11 July 2022

Author(s): ing. L. Kraaijenbrink

Thesis committee:		
	Prof.dr.ir. J.G. Rots	TU Delft
	Prof.dr.ir. M.A.N. Hendriks	TU Delft
	Dr.ir. K.N. van Dalen	TU Delft
	P.J. Flink	Royal HaskoningDHV

Table of Contents

1 Introduction

In this appendix, the treatment of relatively low scaled distances according to the Hopkinson-Cranz scaling law (1.1) are analysed. Detonations with low scaled distances result in a nonlinear pressure distribution over the beam. The reviewed scaled distance is large enough to be considered as far field detonation.

$$Z = \frac{R}{W^{1/3}} \tag{1.1}$$

The investigated experiment is conducted in Hanoi, Vietnam with the purpose of investigating the reliability of the end plate connection (Figure 1.1). The panel (called “Trial 1”) is subjected to the blast generated by 5 kg Ammonite, which is equivalent to 5.5 kg TNT. The explosive material is detonated 2 m away from the panel. This is equivalent to a scaled distance of 1.13 m/kg$^{1/3}$. According to the UFC 3-340-02 (Department of Defence, US, 2008), scaled distances between 0.4 m/kg$^{1/3}$ and 1.2 m/kg$^{1/3}$, could lead to other failure mechanisms than flexural failure. However, the experimental results make clear that flexural failure is the governing failure mechanism.

Figure 1.1: End plate connection

The nonlinear pressure distribution is investigated in more detail in (Wu et al., 2009). In this experiment, two pressure transducers are placed on the beam: one in the middle and the other one near the support. Multiple pressure functions are used in the research, varying in scaled distance, concrete compressive strength, and additional strengthening measures. The beam (called “NRC-2”) is tested on a charge weight of 8 kg and standoff distance of 3 m us used to investigate the influence of a nonlinear pressure distribution. This corresponds with a scaled distance of 1.5 m/kg$^{1/3}$.

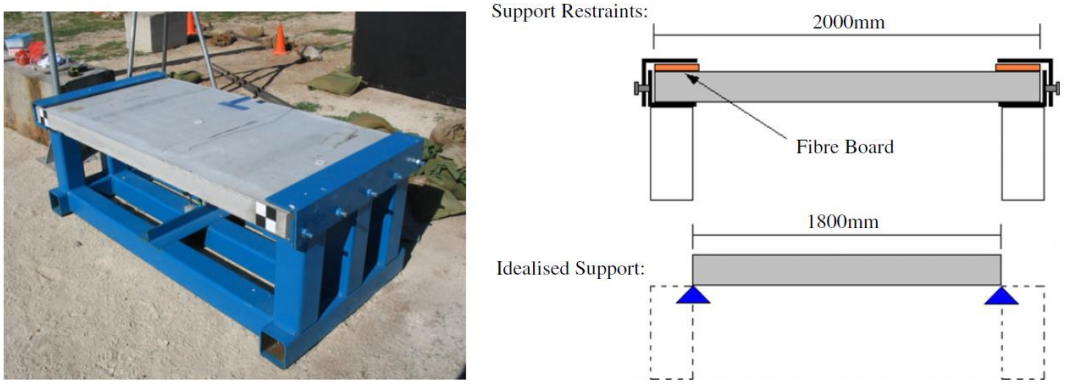

Figure 1.2

The geometries of the specimens are indicated in Figure 1.3. The reinforcement has a 10 mm concrete cover in both cases.

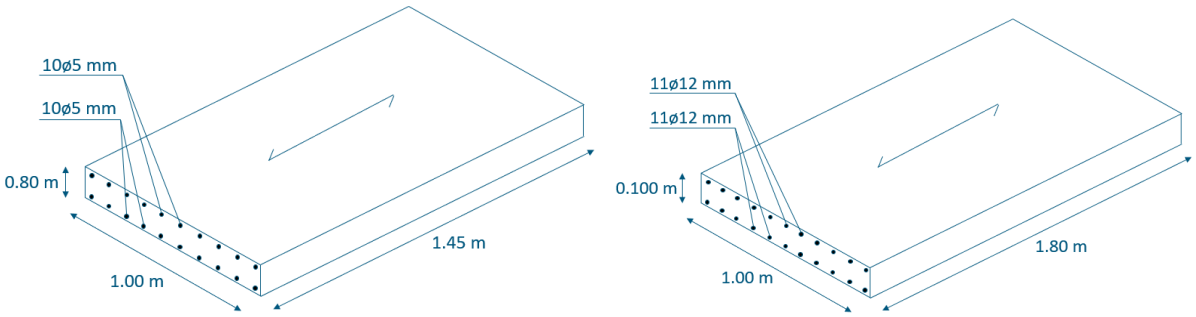

Figure 1.3: specimen geometry of trial 1 (left) and the specimen geometry of NRC-2 (right)

2 Experiment results

The obtained results in the experiments are presented in this chapter. First the beam reported in (Wu et al., 2009) is addressed, followed by the beam reported in (Pham & Ngo, 2015).

2.1 Observations

There is no displacement-time history graph available for either of the beams. The following observations are made for NRC-2:

- A maximum deflection of 10.5 mm is captured with a high-speed camera.
- No cracks are observed

The following observations are made for Trial 1:

- The maximum inwards displacement relative to the support is measured at 35 mm and the maximum outwards displacement of 10 mm
- Three crack lines are observed at the bottom and one crack line at the top, with the most severe crack in the middle.
- The average crack with is 2.6 mm

The concrete panel after the blast trial is shown in Figure 2.1.

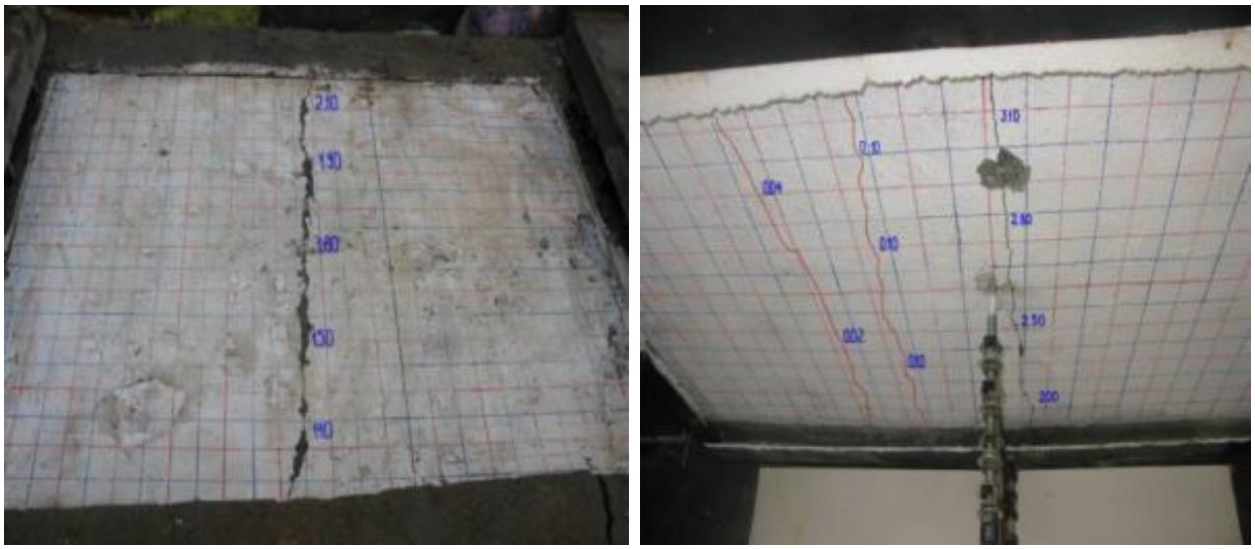

Figure 2.1: concrete panel after the blast, trial 1. Top side on the left and bottom side on the right.

3 Parameters

The parameters in the dynamic analysis are strain rate dependant. The strain rate is extracted from the analyses. An average value for the strain rate is used according to (3.1) and (3.2), where t_E is the time to yield the reinforcement bars. Table 3.1

$$\dot{\varepsilon}_{c,avg} = 0.002/t_E \quad (3.1)$$

$$\dot{\varepsilon}_{s,avg} = f_{dy}/(E_s t_E) \quad (3.2)$$

Table 3.1: Dynamic parameters

Parameter	Units	NRC-2	Trial 1
Time to yield t_E	s	0.010*	0.002
Concrete strain rate $\dot{\varepsilon}_{c,avg}$	s^{-1}	0.20	1.00
Steel strain rate $\dot{\varepsilon}_{s,avg}$	s^{-1}	0.33	1.75
DIF_c	-	1.23	1.28
DIF_t	-	1.43	1.51
DIF_E	-	1.26	1.31
DIG_{GF}	-	1.00	1.00
DIF_{GC}	-	1.23	1.28
*The reinforcement in NRC-2 does not yield. An interpolation is made as follows: $\varepsilon_{sy}/\varepsilon_{s,u,max}*t_{u,max}$			

The concrete properties are included in Table 3.2.

Table 3.2: Concrete properties

Parameter	Units	NRC-2	Trial 1
Young's modulus (static / dynamic)	MPa	28300 / 35658	36487 / 47798
Initial Poisson's ratio	-	0	0
Mass density	Kg/m^3	2400	2400
Tensile curve	-	Hordijk	Hordijk
Tensile strength (static/dynamic)	MPa	8.2 / 11.7	3.85 / 5.82
Fracture energy	N/m	141	150
Compression curve	-	Parabolic	Parabolic
Compressive strength	MPa	39.5 / 48.6	54 / 69.1
Compressive fracture energy	N/m	35371 / 43507	37419 / 47896

The ultimate strength and ultimate strain of the reinforcement applied in NRC-2 is not specified. However, it is known that the reinforcement will not yield in the analysis. Therefore, specifying the ultimate strength and ultimate strain of the reinforcement is unnecessary for NRC-2. The dynamic value for the yield stress is estimated.

All the static parameters of trial 1 in Table 3.3 are given in (Pham, 2015). The dynamic values are estimated.

Table 3.3: Steel reinforcement properties

Parameter	Units	NRC-2	Trial 1
Young's modulus	MPa	200000	200000
Yield stress (static / dynamic)	MPa	600 / 650	630 / 730
Ultimate engineering stress (static / dynamic)	MPa	600 / 650	660 / 730
Ultimate engineering strain	-	-	0.144

The applied concrete and reinforcement stress-strain relationships are shown in Figure 3.1 and Figure 3.2.

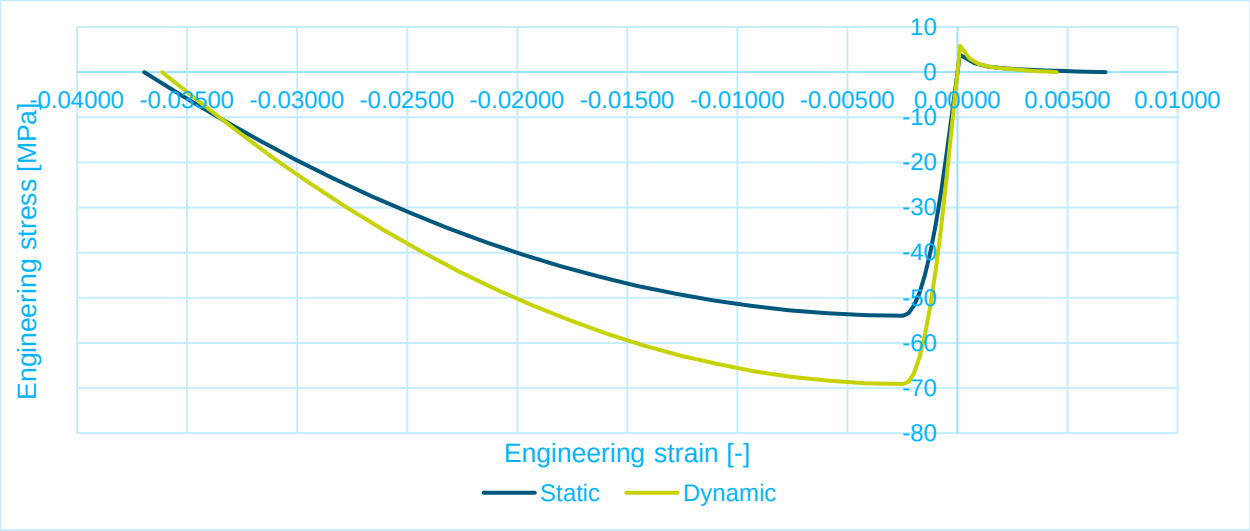

Figure 3.1: Concrete stress-strain relationship for the element length of 30.21 mm

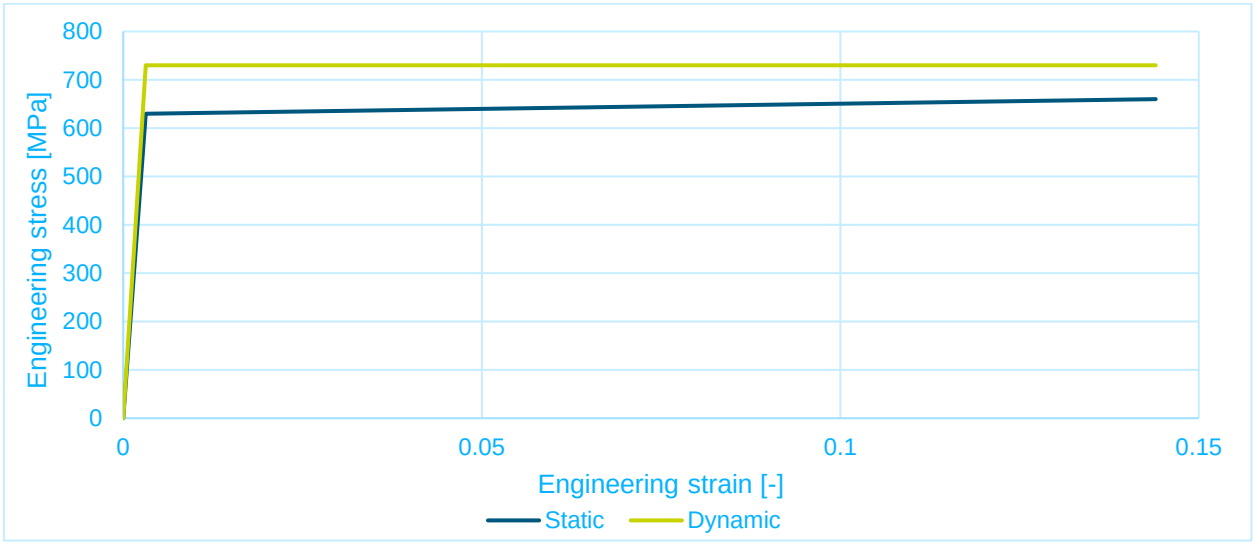

Figure 3.2: Reinforcement stress-strain relationship for Trial 1

4 Applied force

The force applied to NRC-2 is measured at two locations: in the middle and near the support (

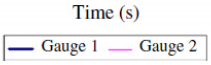

Figure 4.1). The measured peak reflected overpressure for PT1 and PT2 are 2.39 MPa and 1.0 MPa, respectively. The reflected pressures for PT1 and PT2 are 0.715 MPa*ms and 0.514 MPa*ms, respectively.

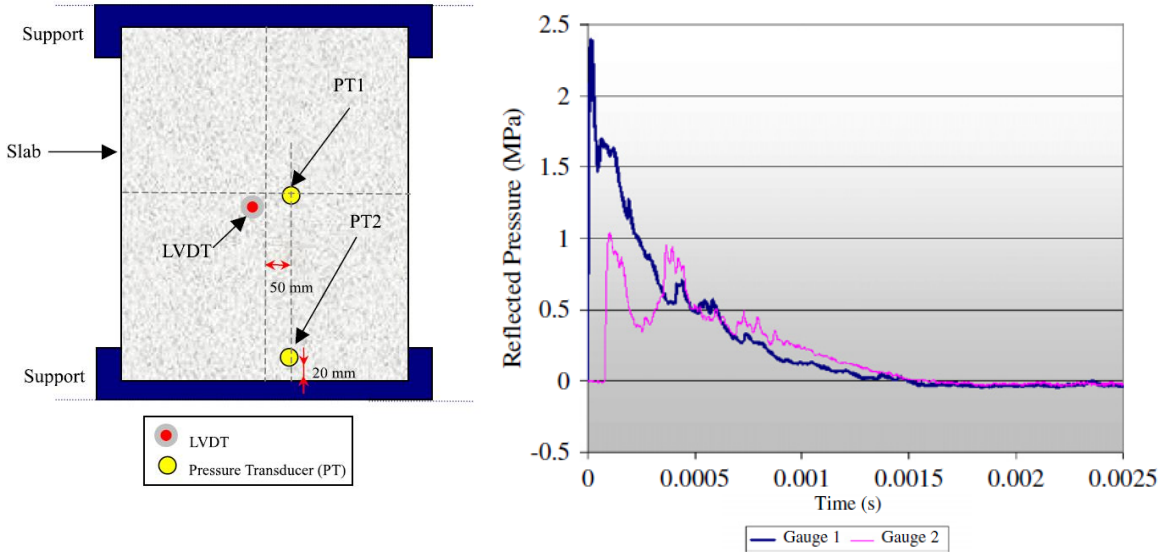

Figure 4.1: Measured pressure on NRC-2

The pressure on the beam is approximated by the scheme in Figure 4.2. This does not exactly represent the actual pressure distribution on the beam, but rather approximates it closely.

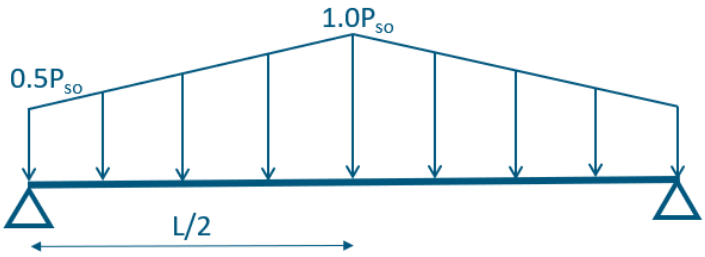

Figure 4.2: simplification of the nonlinear pressure distribution

The applied pressure at PT1 is approximated by (4.1). The parameters for the pressure function are included in Figure 4.3, along side the graph of the approximating pressure function. The parameters are chosen in such a way that the impulse is the same as in (Wu et al., 2009).

$$P_s(t) = 2.1\left(1 - \frac{t}{0.0015}\right)e^{-3\frac{t}{0.0015}} \tag{4.1}$$

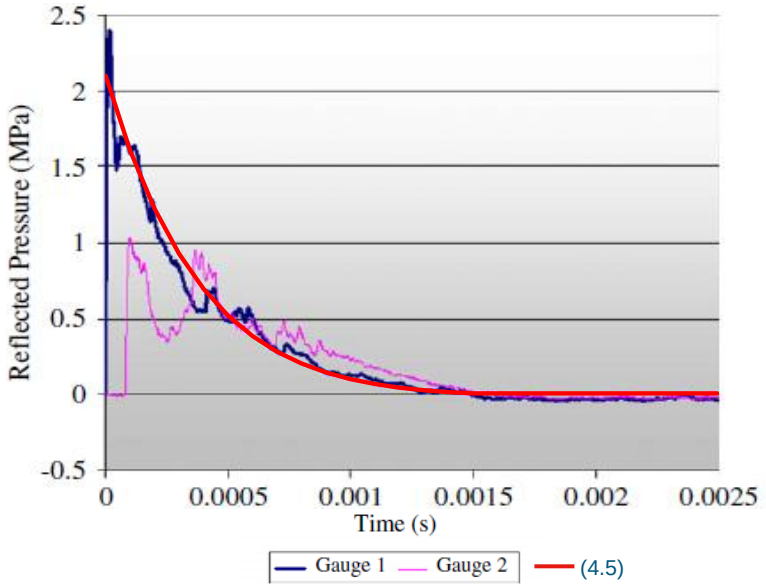

Figure 4.3: Reflected pressure-time history graph for NRC-2

The reflected pressure-time history graph of trial 1 is shown in Figure 4.4. the applied pressure is approximated by (4.2)

$$P_s(t) = \begin{cases} 16000t - 6400 & \text{for } 0.4 \text{ ms} \leq t \leq 0.55 \text{ ms} \\ 2400\left(1 - \dfrac{t}{0.0015}\right)e^{-4.5\frac{t}{0.0015}} & \text{for } 0.55 \text{ ms} < t \leq 2.05 \text{ ms} \end{cases} \quad (4.2)$$

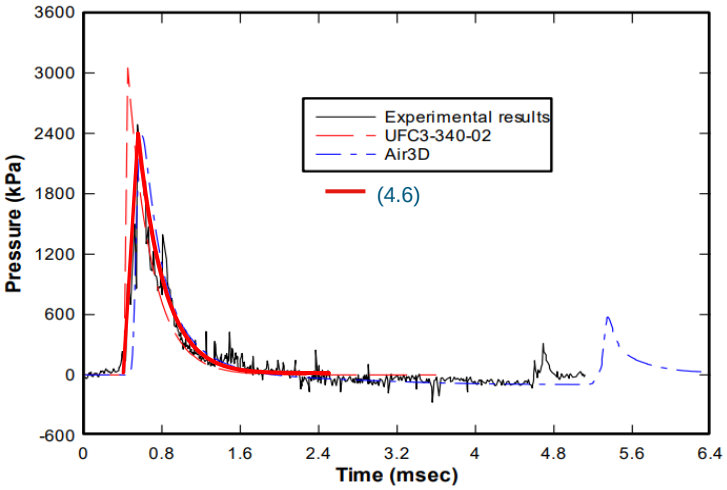

Figure 4.4: Reflected pressure-time history graph for Trial 1

5 Dynamic analysis with FEM comparison

In this chapter, the results of the FDM analyses are presented. A comparison is made with the FEM results.

5.1 Moment curvature relationship

The M-κ graph is manually constructed and shown Figure 5.1 and Figure 5.2. The M-κ graphs are more specified in Table 5.1. Especially the M-κ graph for trial 1 (Figure 5.2) is interesting. The first dip indicates cracking. The second dip is where the reinforcement is yielding.

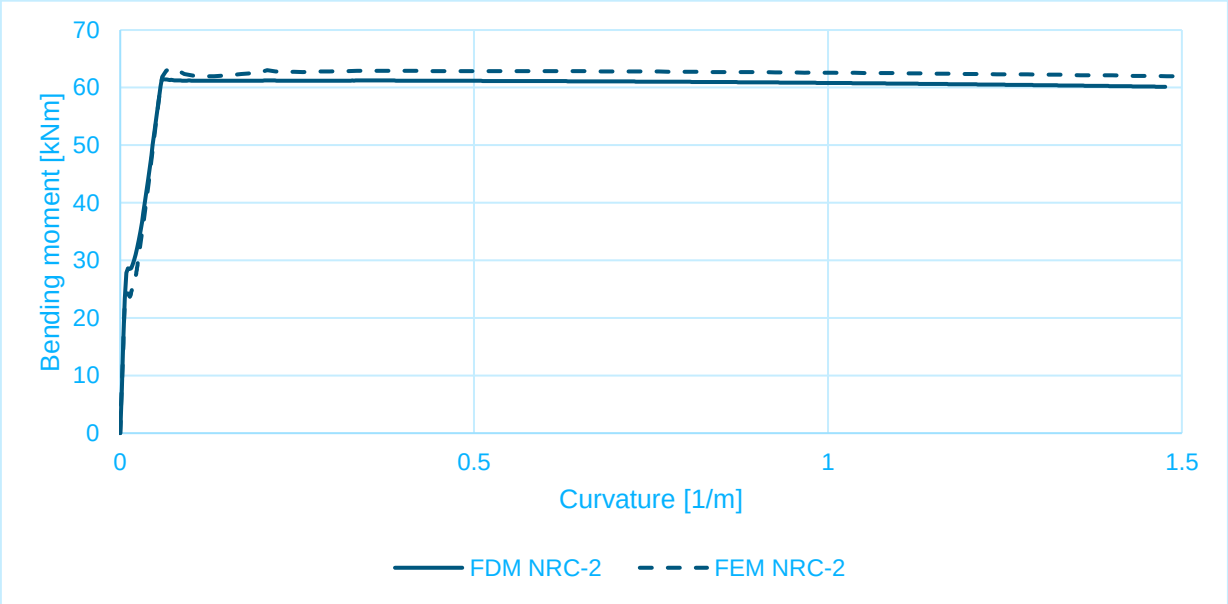

Figure 5.1: M-κ graph for NRC-2

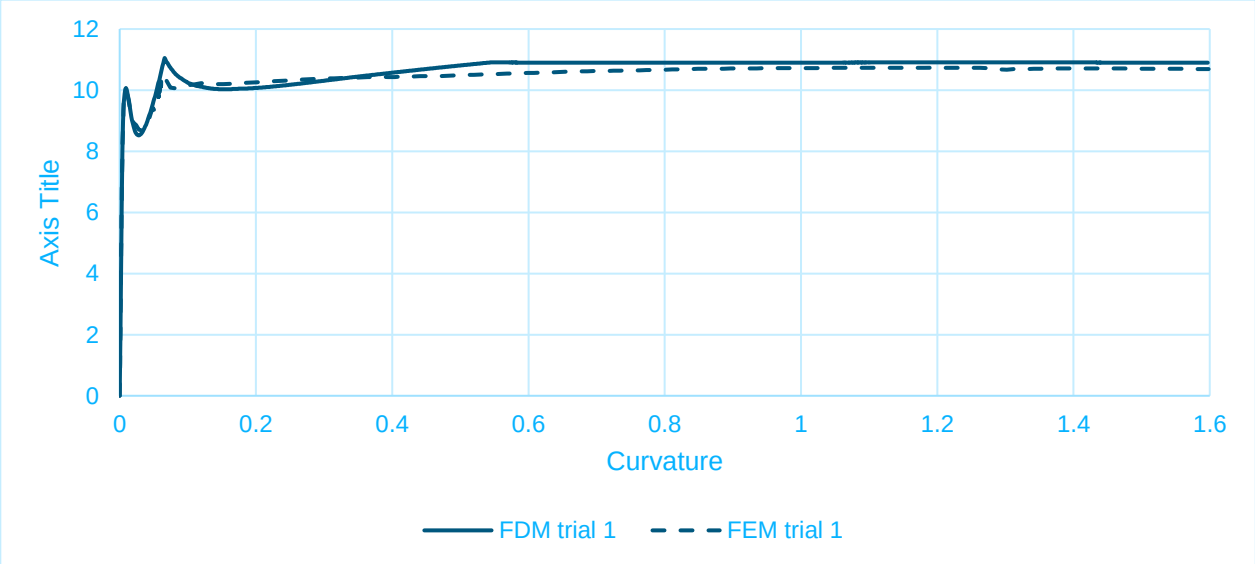

Figure 5.2: M-κ graph for Trial 1

Table 5.1: Distinct points in the M-κ graph

	Units	NRC-2	Trial 1
Cracking bending moment	kNm	23.29	6.39
Cracking curvature	1/m	0.00656	0.00304
Yielding bending moment	kNm	60.32	9.88
Yielding curvature	1/m	0.0569	0.00710
Ultimate bending moment	kNm	61.52	10.91
Ultimate curvature	1/m	1.477	1.597

5.2 Force-displacement relationship

The force-displacement (F-u) graph for NRC-2 is shown in Figure 5.3 and for Trial 1 in Figure 5.4. The F-u graphs are more specified in Table 5.2. The FEM analysis is force-controlled with arc-length turned on. This allows for local dips in the F-u graph. The FDM model is force-controlled without arc-length. Especially for trial 1, this limits the accuracy of the F-u graph. The geometry of trial 1 is not realistic for actual slab in a building. The F-u graph for a slab in a building would look like the one for NRC-2.

When the deflection changes direction, the cracks are closed on initial tension side and could appear on the other side of the beam. It is not clear what the stiffness of the beam is when the cracks are closed (unloading stiffness). Therefore, three ways of specifying the unloading stiffness are considered. They are indicated in Figure 5.5.

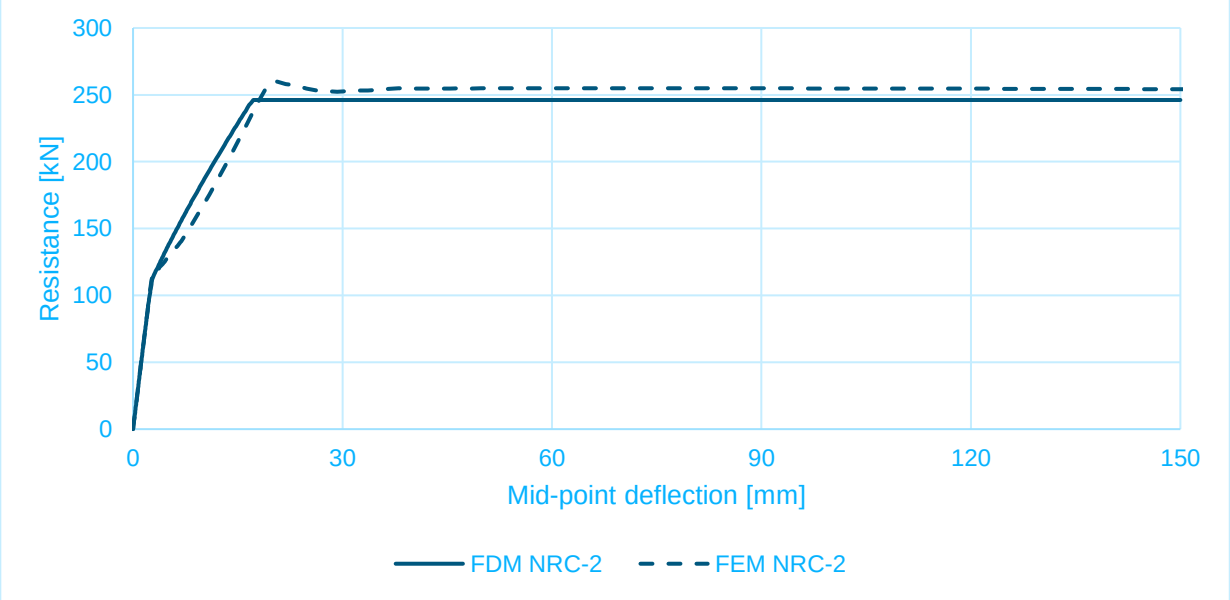

Figure 5.3: F-u graph for NRC-2

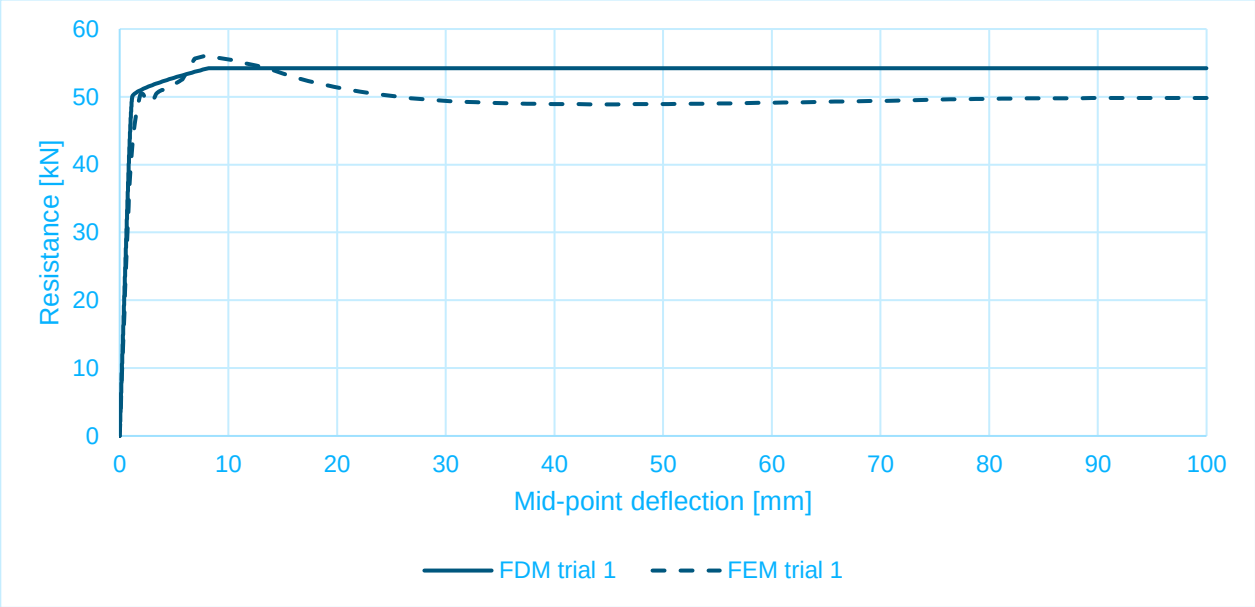

Figure 5.4: F-u graph for Trial 1

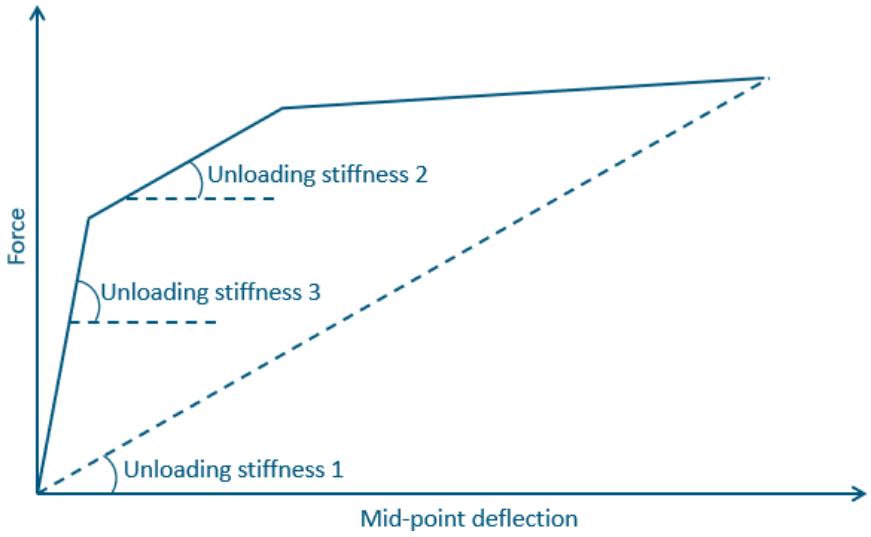

Figure 5.5: Unloading stiffnesses

Table 5.2: Distinct points in the F-u graph

	Units	NRC-2	Trial 1
Cracking force	kN	93.53	31.76
Cracking deflection	mm	2.19	0.658
Yielding force	kN	246.14	49.88
Yielding deflection	mm	6.22	1.14
Ultimate force	kN	246.14	54.21
Ultimate deflection	mm	--	--

5.3 Single degree of freedom mass-spring system

The load is more concentrated on the middle of the beam, leading to a different load factor and mass factor. This is demonstrated in equations (5.1), (5.2), (5.3), and (5.4), where the static case is evaluated. The load factor and mass factor for a distributed load are 0.64 and 0.50, respectively.

$$P(x, P_{so}) = \frac{P_{so}}{2} + \frac{P_{so}}{2}\frac{2x}{L} \tag{5.1}$$

$$\phi(x) = \frac{2x(16x^4 + 40Lx^3 - 120L^2x^2 + 65L^4)}{41L^5} \tag{5.2}$$

$$K_L = \frac{\int_0^{L/2} P(x, P_{so} = 1)\phi(x)\, dx}{\int_0^{L/2} P(x, P_{so} = 1)\, dx} = 0.696 \tag{5.3}$$

$$K_M = \frac{\int_0^{L/2} \phi(x)^2\, dx}{L/2} = 0.502 \tag{5.4}$$

The load factor and mass factor for NRC-2 are given in Figure 5.6 and for Trial 1 in Figure 5.7.

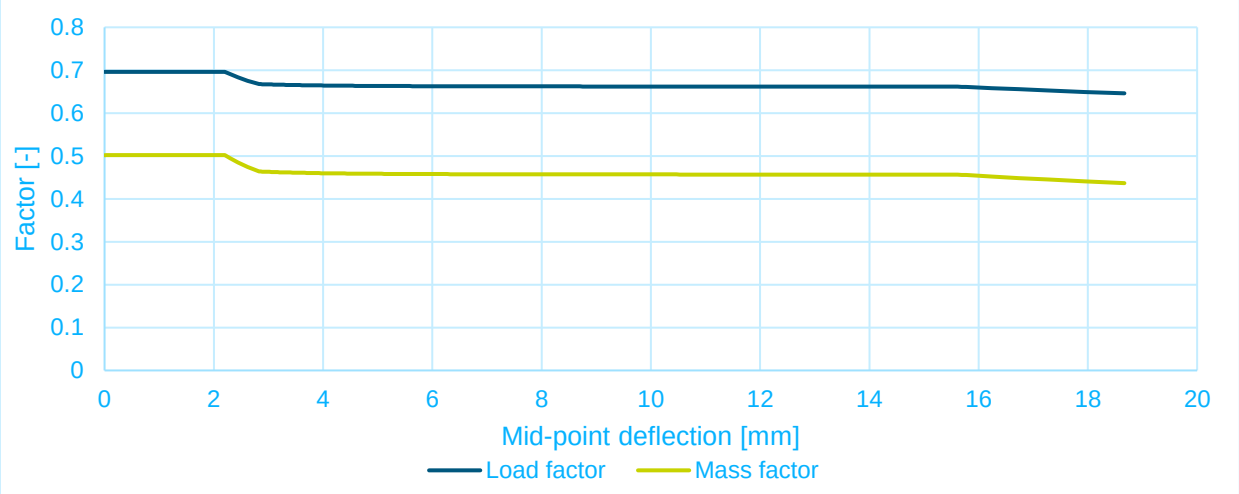

Figure 5.6: mass factor and load factor for NRC-2

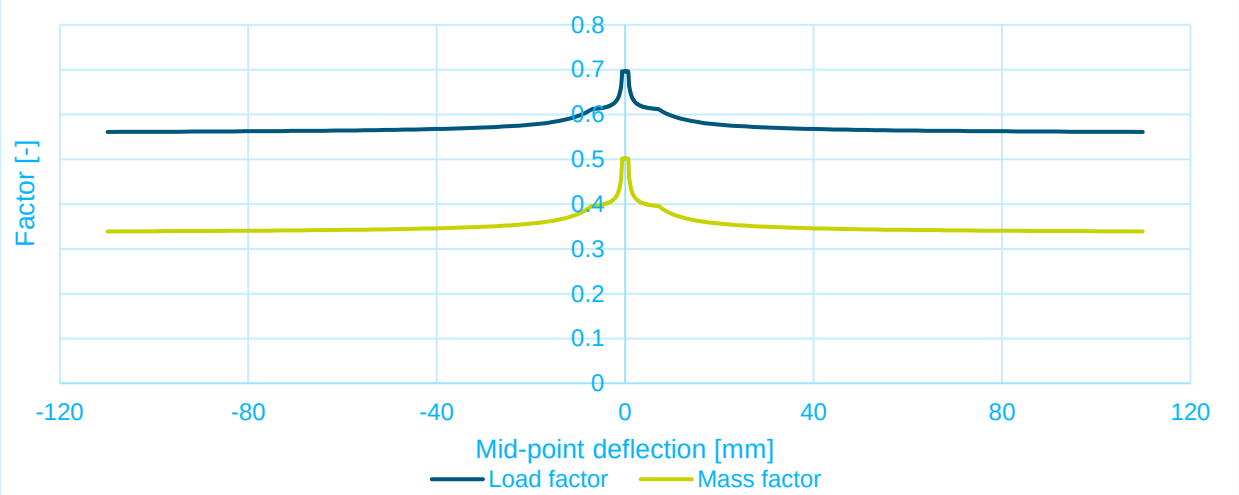

Figure 5.7: mass factor and load factor for Trial 1

The results of the mass-spring system analyses are shown in Figure 5.8 and Figure 5.9. Both beams are in good agreement with the experimental results.

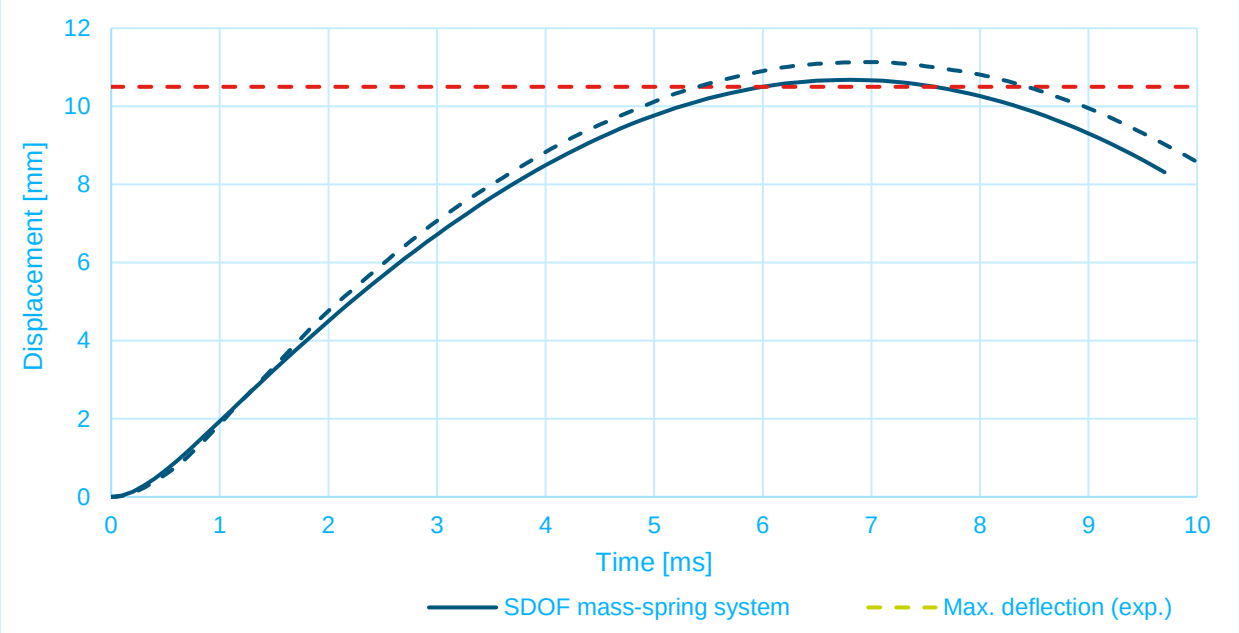

Figure 5.8: Mass-spring system deflection for NRC-2

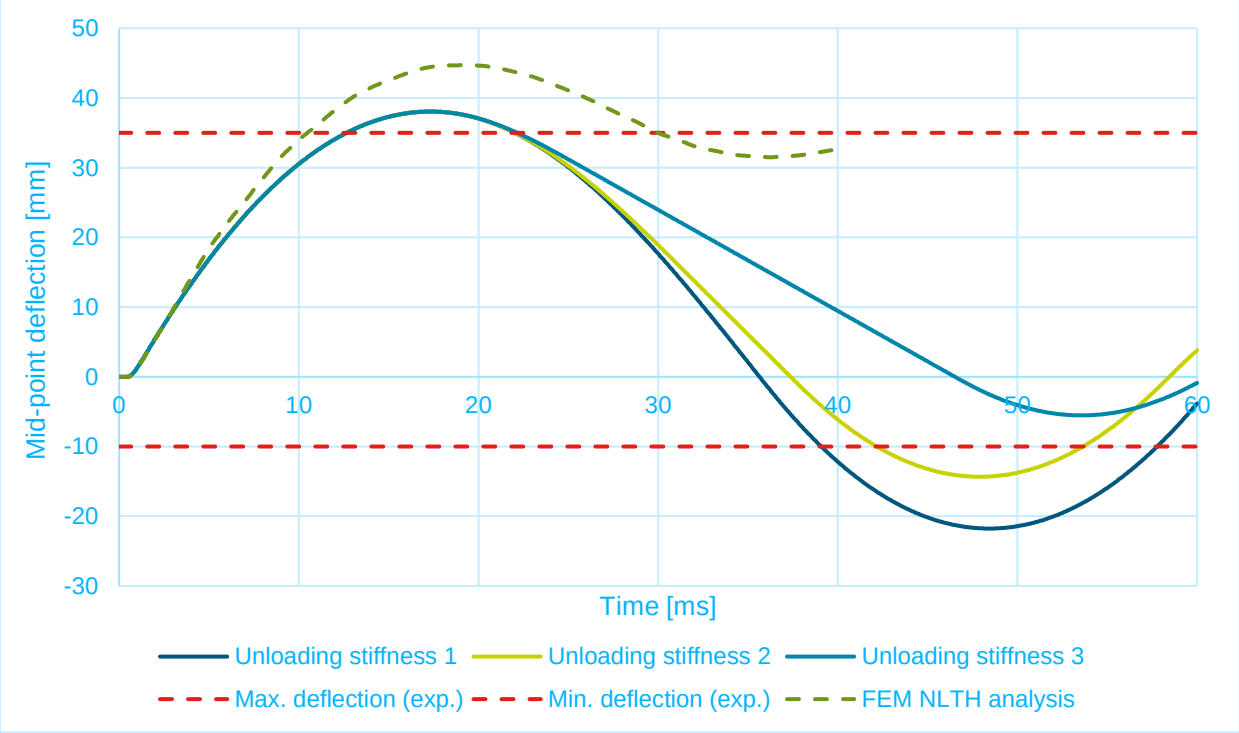

Figure 5.9: Mass-spring system deflection for Trial 1

The spring force throughout the Trial 1 analysis are given in Figure 5.10 and Figure 5.11. Figure 5.10 compares the F-u graph for the beam with the one for the mass-spring system (multiplied by the load factor). Figure 5.11 compares the different unloading stiffnesses that are analysed.

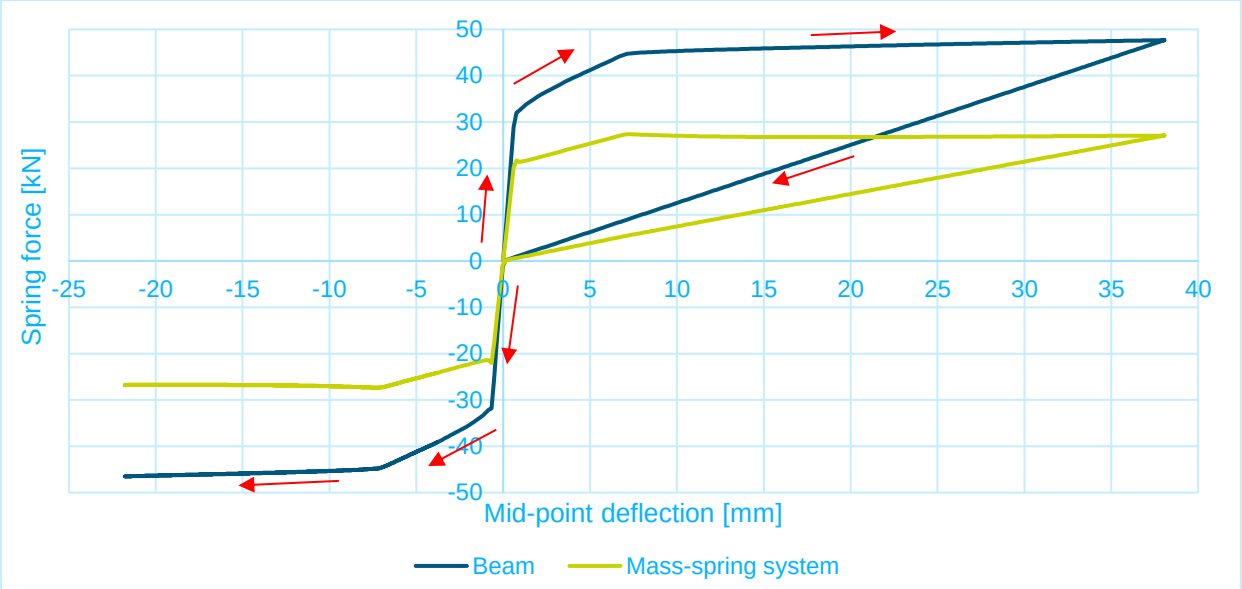

Figure 5.10: Spring force path throughout the analysis

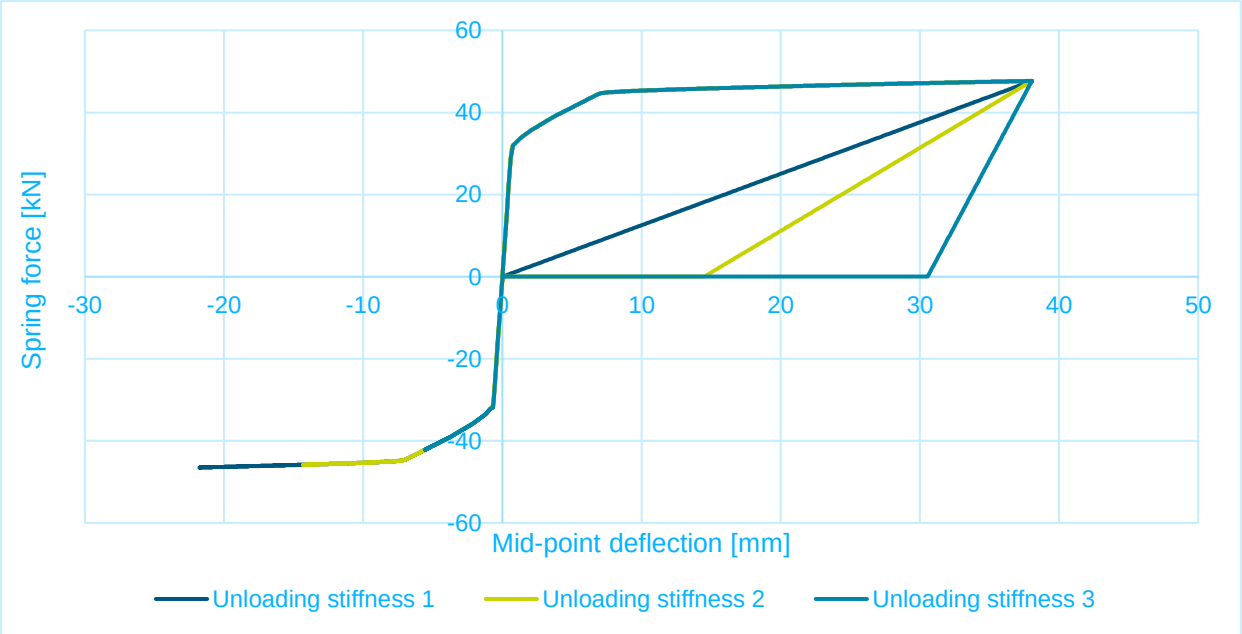

Figure 5.11: Spring force paths for different unloading stiffnesses

6 Discussion

UFC 3-340-02 considers scaled distances above 1.2 m/kg$^{1/3}$ explosions in the ‘far field’ design range. This does not necessarily mean that blast load categorised in the far field design range leads to a uniform pressure distribution. This is showed in (Wu et al., 2009), where the pressure is measured in the middle of the beam and near the support. These pressure measurements are used to predict the pressure distribution for the beam reported in (Pham & Ngo, 2015).

The load is more concentrated on the middle of the beam, leading to a different load factor and mass factor. This is demonstrated in equations (5.1), (5.2), (5.3), and (5.4), where the static case is evaluated.

The load factor and mass factor for a triangular load as shown in Figure 4.2 are 0.696 and 0.502, respectively. For a distributed load, these factors are 0.64 and 0.50.

Three ways of specifying the unloading stiffness are considered and compared. The influence of the unloading stiffness is made clear in Figure 5.9. Based on this research, the unloading path 2 is the best choice. For unloading stiffness 2, the deflection is slightly overestimated for the maximum inwards and maximum outwards deflection. It should be noted that this requires more in-depth research for better insight in the unloading branch.